ACCOUNTS
of chemical research

Exciton−Exciton Correlations Revealed by Two-Quantum, Two-Dimensional Fourier Transform Optical Spectroscopy

KATHERINE W. STONE,[†] DANIEL B. TURNER,[†] KENAN GUNDOGDU,[†,§] STEVEN T. CUNDIFF,[‡] AND KEITH A. NELSON*[,†]

[†]*Department of Chemistry, Massachusetts Institute of Technology, Cambridge, Massachusetts 02139,* [‡]*JILA, University of Colorado, Boulder, and National Institute of Standards and Technology (NIST), Boulder, Colorado 80309*

RECEIVED ON MAY 4, 2009

Downloaded by RENMIN UNIV OF CHINA on October 2, 2009 | http://pubs.acs.org
Publication Date (Web): August 19, 2009 | doi: 10.1021/ar900122k

CONSPECTUS

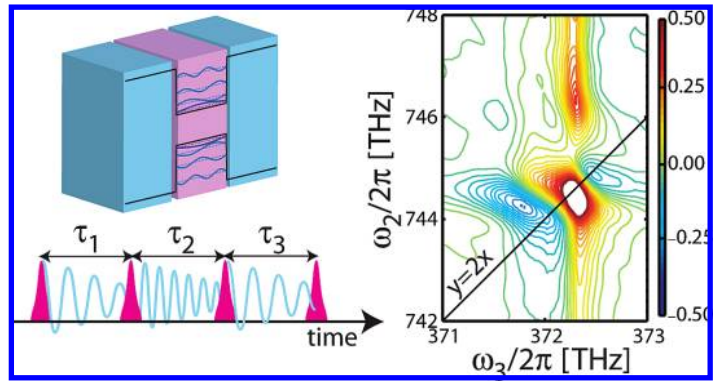

The Coulomb correlations between photoexcited charged particles in materials such as photosynthetic complexes, conjugated polymer systems, J-aggregates, and bulk or nanostructured semiconductors produce a hierarchy of collective electronic excitations, for example, excitons, and biexcitons, which may be harnessed for applications in quantum optics, light-harvesting, or quantum information technologies. These excitations represent correlations among successively greater numbers of electrons and holes, and their associated multiple-quantum coherences could reveal detailed information about complex many-body interactions and dynamics. However, unlike single-quantum coherences involving excitons, multiple-quantum coherences do not radiate; consequently, they have largely eluded direct observation and characterization.

In this Account, we present a novel optical technique, two-quantum, two-dimensional Fourier transform optical spectroscopy (2Q 2D FTOPT), which allows direct observation of the dynamics of multiple exciton states that reflect the correlations of their constituent electrons and holes. The approach is based on closely analogous methods in NMR, in which multiple phase-coherent fields are used to drive successive transitions such that multiple-quantum coherences can be accessed and probed. In 2Q 2D FTOPT, a spatiotemporal femtosecond pulse-shaping technique has been used to overcome the challenge of control over multiple, noncollinear, phase-coherent optical fields in experimental geometries used to isolate selected signal contributions through wavevector matching. We present results from a prototype GaAs quantum well system, which reveal distinct coherences of biexcitons that are formed from two identical excitons or from two excitons that have holes in different spin sublevels ("heavy-hole" and "light-hole" excitons). The biexciton binding energies and dephasing dynamics are determined, and changes in the dephasing rates as a function of the excitation density are observed, revealing still higher order correlations due to exciton−biexciton interactions. Two-quantum coherences due to four-particle correlations that do not involve bound biexciton states but that influence the exciton properties are also observed and characterized.

The 2Q 2D FTOPT technique allows many-body interactions that cannot be treated with a mean-field approximation to be studied in detail; the pulse-shaping approach simplifies greatly what would have otherwise been daunting measurements. This spectroscopic tool might soon offer insight into specific applications, for example, in detailing the interactions that affect how electronic energy moves within the strata of organic photovoltaic cells.

Published on the Web 08/19/2009 www.pubs.acs.org/acr
10.1021/ar900122k CCC: $71.50 © 2009 American Chemical Society

Downloaded by RENMIN UNIV OF CHINA on October 2, 2009 | http://pubs.acs.org
Publication Date (Web): August 19, 2009 | doi: 10.1021/ar900122k

Introduction

Correlated electronic motions affect significantly the coherent optical responses of assemblies of molecular chromophores and semiconductor nanostructures. In biological light-harvesting complexes, singly excited states belonging to the constituent chromophores are coupled coherently to each other.[1] Furthermore, multiply excited states may have evolved in order to provide rapid relaxation pathways after absorption of highly energized photons in order to avoid damage.[2] Multiply excited states in semiconductor quantum dots may play key roles in optical gain and have been suggested for harnessing the extra energy deposited in these materials by the absorption of highly energetic photons.[3]

A two-particle interaction between an optically excited electron and a positively charged hole forms a bound quasiparticle (an exciton) with energy ε_e. The range of the mediating Coulomb force is long, so the behavior of excitons may be influenced by higher-order correlations that arise through interactions with other multiple-particle complexes such as excitons or unbound electron−hole pairs. Thus, spectroscopically measured optical responses can be described by the coherent motions of a hierarchy of multiple-particle correlations. At the level of four-particle correlations, a pair of excitons may form a bound quasiparticle known as a biexciton. The energy of the biexciton state, ε_b, differs from the sum of energies of the exciton states by the biexciton binding energy, Δ. Biexciton coherent behavior (scattering mechanisms, decoherence rates, etc.) is relevant to coherent control schemes[4] for quantum information processing.[5] In another instance of four-particle correlations, an exciton may scatter from another bound or unbound electron−hole pair. From early optical four-wave mixing (FWM) experiments[6,7] on semiconductor quantum wells (QWs), it was evident that the oscillation frequency, $\omega_e = \varepsilon_e/\hbar$, and dephasing rate, γ_e, of exciton coherences were dependent on the excited carrier density, the effects dubbed excitation induced shift (EIS) and excitation-induced dephasing (EID), respectively. These phenomena are discussed in several reviews.[8−10]

Direct spectroscopic investigation of higher-order correlations has proven difficult because the associated multiexciton coherences generally do not radiate since the optical transitions are formally forbidden. Rather, as in the FWM experiments mentioned above, they are probed indirectly through sequential single-quantum transitions. Therefore frequency domain experiments such as photoluminescence[11] and spectrally resolved FWM measurements[12] in semiconductor QWs may reveal biexciton energetics and some dephasing information if the biexciton binding energy is larger than the low-temperature exciton line width.

High-order *nuclear spin* coherences have been isolated and observed through multiple-quantum techniques[13] used in two-dimensional Fourier transform nuclear magnetic resonance (2D FTNMR) spectroscopy. Higher-order electronic correlations, such as biexciton coherences, could be observed through an optical analog to two-quantum 2D FTNMR, that is, two-quantum 2D Fourier transform optical spectroscopy (2D FTOPT). However, performing these experiments requires that all the fields have controlled phase relationships. In the infrared (IR) spectral region, the wavelength is long enough to meet this requirement without extraordinary measures, and two-quantum 2D FTIR of molecular vibrational overtones has been demonstrated.[14] Phase-coherent 2D FTOPT can be conducted using a collinear beam geometry,[15] but in that case, only the absorptive part of the 2D spectrum is detected. The use of a noncollinear phase-matched geometry allows background-free detection of the full signal, but maintaining phase coherence among multiple beams with variable time delays presents significant experimental challenges, which we have addressed as described below.

Here we present two-quantum 2D FTOPT spectroscopy measurements on GaAs/AlGaAs QWs, which separate four-particle correlations, such as biexcitons, from lower-order correlations observed typically in conventional 2D FTOPT experiments on semiconductors[16] and photosynthetic antenna complexes.[1] Our measurements of higher-order correlations involving the "heavy-hole" exciton complement the "S3" measurements presented by Cundiff et al.[17] in this issue. In addition, we observe higher-order correlations of mixed character including the "light−hole" exciton. We also observe a change in the real 2D line shape of features originating from biexciton−ground-state coherences when using perpendicularly polarized excitation fields that indicates suppression of other four-particle correlations as described below. The following section describes higher-order correlations and the specific types of exciton interaction phenomena observed in the coherent nonlinear optical response of semiconductors. Then we describe the spatiotemporal femtosecond pulse shaping technique used to perform two-quantum 2D FTOPT measurements, and we discuss the biexciton energetics and dephasing dynamics revealed in the absolute and complex 2D spectra recorded with different excitation intensities and polarizations.

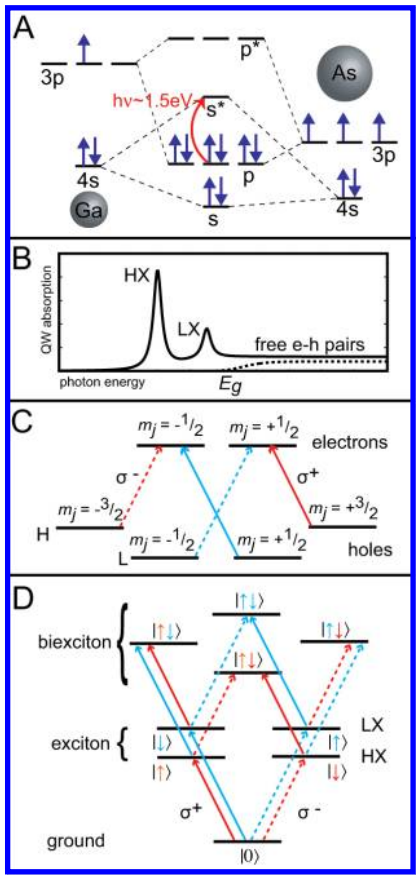

FIGURE 1. (A) Semiconductor energy level diagram in the electron/hole representation showing the origin of different exciton states based on the underlying atomic orbital and spin states. (B) Illustrative linear absorption spectrum of a semiconductor QW with (solid) and without (dashed) Coulomb interactions. Free electron−hole pairs absorb photons with energy higher than the bandgap, E_g. Coulombic nonlinearities increase their absorption coefficient and create bound quasiparticle exciton states, labeled HX and LX, which absorb below E_g. (C) Expanded view of p and s* states from which excitons are formed. The excited electron is in an s-type state with degenerate spin sublevels $m_j = \pm 1/2$. The hole is in a p-type state with spin sublevels $m_j = \pm 3/2$ and $\pm 1/2$ whose energies are split due to quantum confinement, labeled heavy hole (H) and light hole (L) due to their effective masses. Polarization selection rules for absorption are indicated. (D) Energy level diagram in the exciton representation illustrating the polarization selection rules for HX and LX excitons and biexcitons. Red and blue arrows represent excitation of the HX and LX exciton, respectively. Solid and dashed arrows represent right-hand and left-hand circularly polarized light, respectively.

Exciton Interactions in Semiconductor QWs

Semiconductor QWs are ideally suited for study of many-electron correlations due to their reduced dimensionality and the fact that the interacting carriers can be generated optically at precisely specified times and densities. The electronic energy levels of atoms at different lattice sites combine to form the collective electronic band states of the material (see Figure 1A). Absorption of a photon excites an electron to the conduction band, leaving a positively charged hole in the valence band. The Coulomb interactions between these charged carriers changes the linear absorption spectrum of a semiconductor, such that below the bandgap strong narrow absorption lines are observed and indicate the formation of correlated (bound) electron−hole pairs, that is, excitons (see Figure 1B). Confinement enhances the binding energy of excitons and biexcitons in semiconductor nanostructures and splits the degenerate spin−orbit coupling states of the valence band, labeled heavy-hole (HH) and light-hole (LH) according to their effective masses. Polarization selection rules for photon absorption for hole and electron states at the valence and conduction band edges are shown in Figure 1C. Biexciton states are displayed more conveniently in a quasiparticle picture, Figure 1D, where three tiers of states represent the sample with increasing levels of collective excitation: the ground state (no excitation), the exciton states, X (one-quantum excitations), and the biexciton states, X_2 (two-quantum excitations).

A macroscopic third-order polarization is induced in the QW sample upon excitation with three noncollinear electromagnetic fields $\vec{E}_A$, $\vec{E}_B$, and $\vec{E}_C$ with propagation directions defined by their respective wavevectors $\vec{k}_A$, $\vec{k}_B$, and $\vec{k}_C$. In single-quantum FWM measurements, $\vec{E}_C$ arrives first to generate exciton coherences, and after a variable delay τ_1, interaction with $\vec{E}_A$ produces exciton populations in a transient grating pattern with wavevector $\vec{k}_A - \vec{k}_C$. The polarizations of the fields can be used to select the spin of the exciton population. Right/left cocircularly polarized fields create populations of spin-up/down excitons, while cross-circularly polarized fields do not create any population gratings.

The presence of the exciton population grating diffracts field $\vec{E}_B$, incident at the phase-matching or Bragg angle, to yield the coherently scattered signal $\vec{E}_S$ with wavevector $\vec{k}_S = -\vec{k}_C + \vec{k}_A + \vec{k}_B$. The last field $\vec{E}_B$ also reverses the temporal phases of the exciton coherences that evolved during τ_1 such that the decay of $\vec{E}_S(\tau)$ yields the homogeneous dephasing time since any inhomogeneous dephasing due to local variation in the frequency is reversed due to the "rephasing" imparted by $\vec{E}_B$. Alternatively, field $\vec{E}_A$ may arrive first to generate exciton coherences, followed by field $\vec{E}_C$, which interacts to form the exciton population grating. In this case, the last field $\vec{E}_B$ does not reverse the temporal phase of the exciton coherences excited by $\vec{E}_A$. We used these so-called "nonrephasing" measurements to obtain the exciton coherence frequency, ω_e, which evolved during τ_1 in order to compare it to the two-quantum coherent oscillations, which evolved dur-

Downloaded by RENMIN UNIV OF CHINA on October 2, 2009 | http://pubs.acs.org
Publication Date (Web): August 19, 2009 | doi: 10.1021/ar900122k

Downloaded by RENMIN UNIV OF CHINA on October 2, 2009 | http://pubs.acs.org
Publication Date (Web): August 19, 2009 | doi: 10.1021/ar900122k

ing τ_2, that we measured using two-quantum 2D FTOPT spectroscopy.

With respect to the rephasing and non-rephasing experiments described above, no signal should be possible if $\vec{E}_A$ and $\vec{E}_B$ arrive at the sample before $\vec{E}_C$ because a population grating at wavevector $\vec{k}_A - \vec{k}_B$ does not diffract field $\vec{E}_C$ in the signal direction. However, signal was observed in two-beam measurements with fields $\vec{E}_A$ and $\vec{E}_B$ combined into one pulse,[18] and higher-order correlations were soon recognized as the cause.[19] In these (1D) measurements, several many-body correlations described phenomenologically as local field effects (LFE), excitation-induced dephasing and energy shift effects (EID and EIS, respectively), and biexciton formation gave rise to two-quantum signal contributions that were heavily convolved[20] because they all had dephasing times on the order of 1−2 ps. However, in our fully coherent two-quantum 2D FTOPT measurements, the two-quantum coherent oscillations that occur during time period τ_2 are observed directly through their effects on the phase and amplitude of the signal field $\vec{E}_S(t)$. Fourier transformation of the complex signal allows separation of the LFE, EID, and EIS contributions, which give rise to "interaction-induced" coherences with twice the exciton frequency, $2\omega_e$, and to biexciton coherences with slightly lower frequency $\omega_b = \varepsilon_b/\hbar = 2\omega_e - \Delta/\hbar$ due to the biexciton binding energy, Δ.

The higher-order correlation contributions are excited by the first two fields, $\vec{E}_A$ and $\vec{E}_B$, which separately excite exciton coherences that oscillate with frequency ω_e and induce macroscopic linear polarization fields, $\vec{P}_A^{(1)}$ and $\vec{P}_B^{(1)}$, in the sample. If the excitation density is high enough, the "local" fields[21] associated with exciton coherences can superpose with the excitation light fields to produce a nonlinear component to the net coherent response that is proportional to the product of the fields and has wavevector $\vec{k}_A + \vec{k}_B$. Thus nearby excitons can be correlated through the local field effects of each one on the other. Higher-order correlations also can result from direct interactions between nearby excitons, without mediation by a local field. As the electrons in nearby electron−hole pairs move away from their parent holes during their coherent oscillation cycles, the screening forces provided by the holes are diminished and the electron−electron repulsions are felt more strongly, leading to motions of the electrons away from each other. This occurs twice during each cycle of the exciton coherences, so the interparticle forces and the particle responses to them oscillate at twice the exciton coherence frequency, $2\omega_e$. The holes also may move alternately farther from and closer to each other at frequency $2\omega_e$ as the screening between them provided by the electrons varies at that frequency. These exciton−exciton interactions give rise to measurable changes in the exciton energy (EIS) and dephasing rate (EID) and are not sensitive to the exciton spin[22] since the spin of electrons does not influence their electrostatic screening. As in the local field case, interactions between excitons that originated from the two different fields $\vec{E}_A$ and $\vec{E}_B$ give rise to two-quantum coherences at a frequency $2\omega_e$ with the sum wavevector $\vec{k}_A + \vec{k}_B$. It has been shown that responses driven by EIS and local field effects are in phase[23] with each other and 90° out of phase with those driven by EID.[24]

As the exciton coherences oscillate, the holes may find new time-averaged locations, forming a bound, four-particle biexciton state whose binding energy is reflected directly in the biexciton coherence oscillation frequency, $\omega_b = 2\omega_e - \Delta/\hbar$. This occurs only between electron and hole pairs of opposite spin as indicated in Figure 1D. Therefore, if $\vec{E}_A$ and $\vec{E}_B$ have opposite circular polarizations, biexciton coherences consisting of two HX or two LX excitons are excited, which we denote as HX_2 and LX_2, respectively. If the fields have the same circular polarization, then biexciton coherences of mixed character (MX_2) consisting of one HX and one LX exciton are excited. Unlike the excitation-induced effects, biexciton coherences are sensitive to exciton spin. In a two-quantum 2D FTOPT measurement, excitation fields $\vec{E}_A$ and $\vec{E}_B$ polarized perpendicularly to the polarization of field $\vec{E}_C$ will only induce biexciton coherences that give rise to coherent scattering of probe light from $\vec{E}_C$ into the signal direction.

While we have described the exciton interaction mechanisms in largely phenomenological terms, four-particle correlations arise naturally in the equations of motion for excitonic wavepackets derived from a many-particle Hamiltonian.[25] Unlike previous FWM experiments on single quantum dots[26] and quantum wells,[27] our measurements not only track the phase evolutions of two-exciton coherences at optical frequencies but also correlate them to optical one-exciton coherences, allowing the phenomena to be studied even when their signatures cannot be separated spectrally.

Spatiotemporal Pulse Shaping for 2D FTOPT Spectroscopy

Spatiotemporal pulse shaping provides a unique and robust platform for performing nonlinear optical spectroscopy measurements. The optical setup used for our experiments is shown in Figure 2A. A single beam containing femtosecond optical pulses from an unamplified Ti:sapphire laser is focused into a static diffractive optical element with a square lattice pattern. Diffraction into ±1 orders yields four beams arranged on the corners of a square that ultimately provide the four

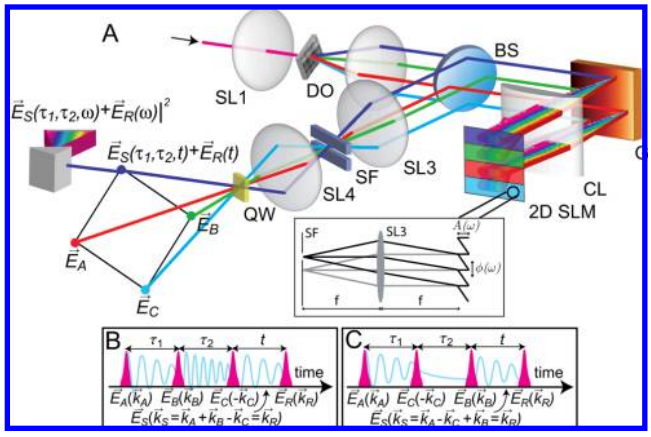

FIGURE 2. (A) Fully coherent 2D FTOPT spectroscopy using a spatiotemporal pulse shaper: (SL1) 10 cm focal length spherical lens, (DO) diffractive optic, (BS) 50/50 beamsplitter, (G) 1400 grooves/mm diffraction grating, (CL) 12.5 cm focal length cylindrical lens, (2D SLM) retro-reflective 2D liquid crystal spatial light modulator, (SF) spatial filter, (SL4) 15 cm focal length spherical lens, and (QW) quantum well sample. The signal emerges from the sample in the wavevector-matching direction, collinear with the reference beam. The illustration shows every optical element before the sample except for wave plates and a neutral density filter in the reference beam. (B) Pulse sequence used to measure two-quantum coherences. The first pulse $\vec{E}_A$ excites exciton coherences that oscillate during τ_1. The second pulse $\vec{E}_B$ converts the exciton coherences to two-exciton coherences, which oscillate during τ_2. A third-order polarization in the sample is induced by the third pulse $\vec{E}_C$, and the signal field $\vec{E}_S(\tau_1,\tau_2,t)$ is radiated during the emission time, t. (C) Pulse sequence used to measure one-quantum exciton coherences.

optical fields for the experiment: $\vec{E}_A$, $\vec{E}_B$, $\vec{E}_C$, and $\vec{E}_R$ with wavevectors $\vec{k}_A$, $\vec{k}_B$, $\vec{k}_C$, and $\vec{k}_R$. This is the familiar "BOXCARS" geometry used in many FWM experiments. The diffractive element and resulting beam pattern are rotated approximately 25° from horizontal such that the four beams are at distinct vertical locations when they are sent into the spatiotemporal pulse shaper, which consists of a grating, cylindrical lens, and 2D spatial light modulator (SLM). The dispersed frequency components of each beam are spread horizontally across a distinct vertical region of the SLM so that pulse shaping of each beam can be executed independently. For each dispersed frequency component of each beam, a vertical sawtooth grating pattern is formed by the SLM pixels, and the spatial phase and amplitude of the pattern are specified to control the optical phase and amplitude of the first-order diffracted light from that component. The diffracted light components are recombined at the grating to generate the four shaped pulses.[28] A very simple "shaping" task is to generate an overall pulse delay. This is achieved by a linear phase sweep of the pulse frequency components with the time delay proportional to $\delta\varphi/\delta\omega$. Thus the FWM experiment can be controlled entirely with the SLM as the only active element. Common-path optics result in minimal phase fluctuations[29] with no need for interferometric monitoring or feedback loops.

The fields $\vec{E}_A$ and $\vec{E}_B$ are used to excite two-quantum optical coherences that result from the higher-order correlations discussed above and that evolve during τ_2. The two-quantum coherence is nonradiative, but the third field, $\vec{E}_C$, which is phase-coherent with the first two fields and the two-quantum coherence they created, produces a new one-quantum coherence, which results in a signal, $\vec{E}_S(\tau_1,\tau_2,t)$, that propagates into the background-free, phase-matched direction $\vec{k}_S = \vec{k}_A + \vec{k}_B - \vec{k}_C$ collinear with the reference field, $\vec{E}_R$. The signal emission and reference fields are superposed in a spectrometer ("spectral interferometry"[30]) and a record of the spectral fringes as a function of ω, which have a periodicity proportional to the time delay between the two fields, is accumulated as τ_2 is increased to obtain the complex 2D signal $\tilde{S}(\tau_2,\omega)$ without the need for numerical Fourier transformation over the signal emission time, t. The pulse sequence illustrated in Figure 2B was used with $\tau_1 = 0$, and Fourier transformation of $\tilde{S}(\tau_2,\omega)$ yielded the complex two-quantum 2D FTOPT spectral surfaces $\tilde{S}(\omega_2,\omega)$, which revealed the two-quantum coherences along ω_2 and their associated exciton emission along the ω coordinate. In other experiments, both τ_1 and τ_2 have been varied and 3D spectral solids have been extracted.[31]

The pulse shaper permits relative delay times between pulses to be varied while maintaining the relative optical phase relationships constant. In particular, a reference frequency ω_0 within the spectral bandwidth of the pulse is selected, and its phase in all four fields is held constant by leaving the four corresponding sawtooth grating patterns fixed throughout the experiment. The effect on the signal field, which is centered at the exciton emission frequency ω_e and which is generated primarily through the action of incident field components near that frequency, is to dramatically slow down its phase variation $\Delta\varphi$ as a function of any pulse delay $\Delta\tau$ such that $\Delta\varphi \approx (\omega_e - \omega_0)\Delta\tau$, in contrast to the usual case, $\Delta\varphi \approx \omega_e\Delta\tau$, in which the signal phase is swept through an entire 2π cycle each time a translational delay stage or variable-thickness wedge is used to change the pulse delay by just one optical period. Our method is precisely analogous to rotating frame detection in NMR. It allows data to be recorded with very coarse time delay steps compared with the usual case in which data must be recorded at many delay points within a single optical period in order to elucidate the signal phase behavior. For the experiments presented in this work, we selected the reference frequency $\omega_0 = 368.00$ THz based on careful calibration of the dispersed frequencies of the

Downloaded by RENMIN UNIV OF CHINA on October 2, 2009 | http://pubs.acs.org
Publication Date (Web): August 19, 2009 | doi: 10.1021/ar900122k

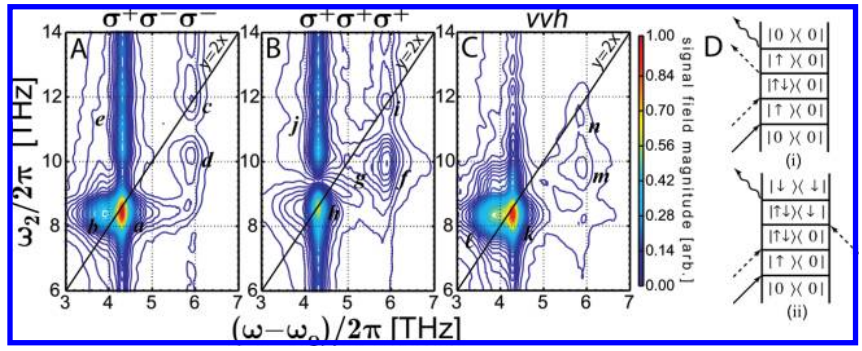

FIGURE 3. Spectral magnitudes of two-quantum 2D FTOPT measurements using (A) cross-circularly, (B) cocircularly, and (C) perpendicularly polarized excitation pulse sequences. The excitation pulse sequence is listed at the top of each spectral surface, so, for instance, in panel A, field $\vec{E}_A$ was right-circularly polarized (σ^+), and fields $\vec{E}_B$ and $\vec{E}_C$ were left-circularly polarized (σ^-). The magnitudes are scaled to the maximum of panel A, and the contour lines are spaced in intervals that are 2% of the maximum. (D) Feynman pathways involving X_2 coherences during τ_2 that emit through (i) an exciton−ground-state coherence or (ii) a biexciton−exciton coherence.

Downloaded by RENMIN UNIV OF CHINA on October 2, 2009 | http://pubs.acs.org
Publication Date (Web): August 19, 2009 | doi: 10.1021/ar900122k

pulses versus horizontal SLM pixel. We confirmed the calibration by measuring the HX coherent oscillation frequency, $\omega_X = 4.35$ THz, in one-quantum measurements, described above and illustrated in Figure 2C, and the quantum well absorption peak at 372.35 THz (not shown).

Several phasing methods have been developed for determining the correct sign of complex one-quantum 2D FTOPT surfaces.[32,33] For our two-quantum surfaces, we may employ the pulse shaper to determine the phase shift between the signal and reference fields by temporally overlapping the time-zero emission signal with the reference pulse and varying the optical phase of one of the excitation fields. This determines the phase offset of the signal field from the reference field, which can be added as a phase shift to one of the excitation pulses during the experiment or multiplied with the entire data set after the measurement.

Results and Discussion

Here we discuss the features in two-quantum 2D FTOPT spectra that indicate direct observation and separation of two-quantum coherences, including biexciton−ground-state coherences. The sample, held at a temperature of 10 K, consisted of 10 layers of 10 nm thick GaAs separated by 10 nm thick $Al_{0.3}Ga_{0.7}As$ barriers. The optically excited carrier density was maintained at or below 10^{11} per cm^2 per well. The energy of the excitation pulses, which had a pulse width of 50 fs, was 18.0 pJ per field, and the center wavelength was 803 nm. The time period τ_2, defined in Figure 2B, was scanned from 0 to 3 ps in 16 fs steps. The reference field propagated through the sample 1.00 ps before emission of the signal was initiated by $\vec{E}_C$, and the reference power was reduced by a factor of 1000 compared with that of the excitation beams. Circular polarizations of the input beams, controlled via individual quarter-wave plates, selected which biexciton and other coherences were observed. A separate quarter-wave plate common to all beams was used in conjunction with the individual wave plates to change the fields to perpendicular polarizations, thereby keeping only the biexciton contributions to the signal.

TABLE 1. Frequency Values (THz) of Peaks from Figure 3 along the ω_2 and ω Axes with Uncertainties That Are 95% Confidence Intervals from Nonlinear Regression to Multiple-Lorentzian Line Shapes[a]

label	two-quantum coherence frequency	one-quantum emission frequency
(a) HX_2	8.45 ± 0.02	4.31 ± 0.00
(b) HX_2−HX	8.45 ± 0.02	3.97 ± 0.02
(c) LX_2	11.87 ± 0.11	5.85 ± 0.02
(d) HX−LX	10.43 ± 0.05	5.85 ± 0.02
(f) MX_2	9.97 ± 0.04	5.87 ± 0.01
(g) MX_2−LX	9.97 ± 0.04	5.47 ± 0.21
(h) HX−HX	8.63 ± 0.04	4.31 ± 0.00
(i) LX−LX	11.68 ± 0.12	5.87 ± 0.01
(k) HX_2	8.35 ± 0.02	4.29 ± 0.00
(l) HX_2−HX	8.35 ± 0.02	3.87 ± 0.02
(m) MX_2	9.79 ± 0.12	5.90 ± 0.05
(n) LX_2	11.47 ± 0.11	5.90 ± 0.05

[a] The user-defined carrier frequency, $\omega_0 = 368.00$ THz, was subtracted from the fitted emission center frequency.

The 2D spectrum determined from the magnitude of the full signal field under cross-circular excitation is displayed in Figure 3A with features denoted *a*−*e*. The positions of features along the two-quantum frequency coordinate, ω_2, and along the emission frequency coordinate, ω, allow us to assign their origins to different exciton interaction phenomena. Peak positions for some of the features labeled in Figure 3, obtained by a least-squares multiple-Lorentzian fit, are listed in Table 1. Note that spectral interferometry detection gives the signal field as a function of the absolute emission frequency, ω, so we have subtracted the carrier frequency, ω_0, from the emission frequency so both coordinates are represented in the rotating frame. The most prominent features (*a* and *b*) centered slightly below the $y = 2x$ line belong to HX_2 coherences. Signal from all two-quantum biexciton coherences

arises through emission by one-quantum exciton coherences through two different pathways, illustrated by the double-sided Feynman diagrams shown in Figure 3D. The final field, $\vec{E}_C$, can either collapse the biexciton−ground-state coherence to a radiative exciton coherence (i) or excite a new exciton coherence (ii) such that the final macroscopic polarization evolves as a biexciton−exciton coherence whose emission is red-shifted along the ω coordinate (*b*). The LX_2 coherence (*c*), about ten times weaker than feature *a* because of the lower LX exciton absorption cross-section, is actually shifted above the $y = 2x$ line probably due to interference with another many-body contribution as discussed further below in connection with Figure 3C. The peak labeled *d* appears along ω_2 at the sum of the HX and LX emission frequencies. Since mixed biexcitons are not expected for cross-circular excitation, this feature results from an interaction-induced two-quantum coherence between HX and LX excitons. The vertical ridges (*e*) along the ω_2 coordinate are due to four-particle correlations, namely, EID,[34] between the excitons and free electron−hole pairs excited by the broadband pulses.

Mixed biexciton coherences (MX_2) are observed in the 2D spectrum, shown in Figure 3B, obtained using cocircular excitation, with features denoted *f*−*j*. The feature belonging to the MX_2 coherence (*f*) appears along the ω_2 axis at a frequency slightly less than the sum of the HX and LX emission frequencies. It also exhibits a red-shifted shoulder (*g*) due to emission from a biexciton−exciton coherence. These features are directly analogous to *a* and *b*, respectively, for the HX_2 biexciton. The peaks labeled *h* and *i* are centered on the $y = 2x$ line and result from two HX and LX excitons, respectively, interacting through EID, EIS, or LFE mechanisms. Again, vertical ridges (*j*) appear along ω_2 that arise due to exciton and unbound electron−hole pair interactions.

Excitation fields polarized perpendicularly to the probe field, $\vec{E}_C$, only induce biexciton coherences. The 2D spectrum for perpendicular excitation is shown in Figure 3C with features denoted *k*−*n*. The HX_2 peak (*k*) and its red-shifted shoulder (*l*) are analogous to *a* and *b* from the cross-circularly polarized data in Figure 3A. The MX_2 peak (*m*) also appears to have a red-shifted feature, but the signal level is too low for the shoulder peak value to be determined reliably. The LX_2 coherence, which results in the peak labeled *n*, is now shifted below the $y = 2x$ line as expected. The vertical ridges that were present in Figure 3A,B are strongly suppressed here, confirming their origin from interaction-induced contributions, as discussed previously.

The peak positions, listed in Table 1, and line widths were determined by fitting multiple Lorentzian functions to the projections along ω_2 and ω of the 2D spectral magnitudes displayed in Figure 3. The spectral projections and their least-squares fits are displayed in Figure 4A,B. Biexciton energetics and dephasing information were obtained from the fitted parameters. The biexciton binding energies, Δ, were determined by subtracting the biexciton coherent oscillation frequency (center frequency in ω_2 from Figure 4A) from the sum of its component exciton coherence frequencies obtained from separate one-quantum measurements. We calculated binding energies of 0.96 ± 0.15 and 1.36 ± 0.26 meV for the HX_2 and MX_2 biexcitons, respectively, using the peak positions of features *a* and *f* from the cross-circular and cocircular excitation measurement, respectively. The binding energies calculated from the peak positions from the perpendicularly polarized excitation measurement for the HX_2 and MX_2 (peaks *k* and *m*) yield binding energies of 1.30 ± 0.13 and 2.08 ± 0.58 meV, respectively, which are slightly larger but just within experimental uncertainties of the other values. The uncertainty in the fitted center frequency for the weak LX_2 peak was too large for the LX_2 binding energy to be determined.

A binding energy also may be extracted from the red-shifted biexciton−exciton emission shoulder (*b*), which may be compared with the exciton−ground-state emission frequency ω_e. A value of 1.38 ± 0.10 meV, similar to those reported earlier,[11,35] was found from the cross-circular polarized data. This value, which might be labeled Δ_{b-e}, differs from the binding energy $\Delta = 0.96$ meV determined from the biexciton−ground-state frequency of feature (*a*),

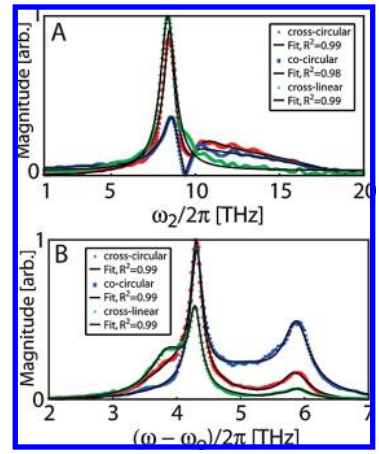

FIGURE 4. Biexciton or exciton−biexciton energetics and dephasing information was obtained by projecting the 2D spectral magnitudes obtained with different excitation polarization to the (A) ω_2 or (B) ω axis and performing a nonlinear least-squares regression using a multiple-Lorentzian fit to the spectral line shape. The fitted center frequencies are given in Table 1. In panel A, the 2D spectrum was only integrated over ω in a range around the HX emission frequency, while in panel B, integration over the entire ω_2 dimension was performed.

Downloaded by RENMIN UNIV OF CHINA on October 2, 2009 | http://pubs.acs.org
Publication Date (Web): August 19, 2009 | doi: 10.1021/ar900122k

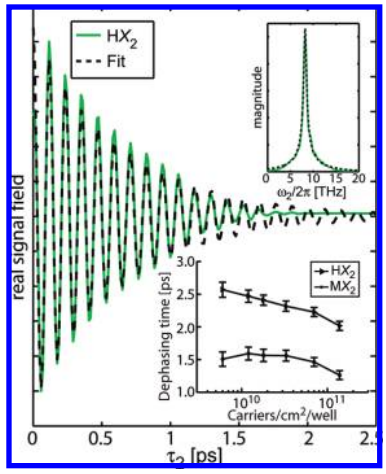

FIGURE 5. HX_2 transient vs τ_2 extracted from the two-quantum 2D FTOPT measurement (shown in Figure 3) where fields $\vec{E}_A$ and $\vec{E}_B$ excited the sample time-coincidentally (i.e., $\tau_1 = 0$) and were collinearly polarized. The oscillations are shifted into the rotating frame. Fourier transform to the ω_2 frequency domain is shown in the upper inset. A single Lorentzian fit (dotted) yielded a center frequency, ω_{HX_2}, of 8.35 ± 0.01 THz and a dephasing time, γ_{HX_2}, of 1.86 ± 0.08 ps. Lower inset: HX_2 and MX_2 biexciton dephasing dependence on the coherently generated carrier density.

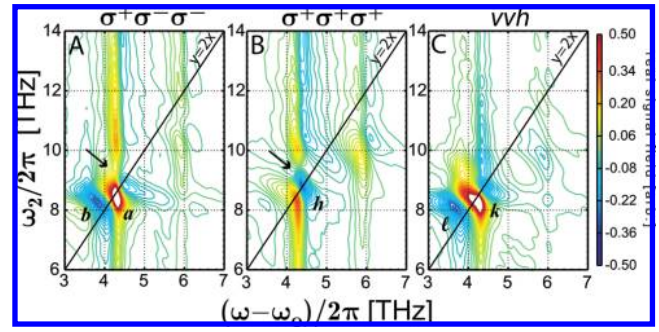

FIGURE 6. Real parts of the complex signal displayed in Figure 3 for (A) cross-circularly, (B) cocircularly, and (C) perpendicularly polarized excitation pulse sequences. The arrows highlight the absence of a phase shift between the (A) HX_2 and vertically elongated features, or as in panel B, the presence of a phase shift between the interaction-induced coherence peak and the vertically elongated feature. Since the vertically elongated feature was previously shown to originate from EID contributions (see main text), the phase shift indicates that the interaction-induced peak is mainly due to EIS contributions.

but these two values represent different properties since Δ_{b-e} is weighted by the transition dipole between subsets of biexciton and exciton configurations. As in the case of Δ, the value of Δ_{b-e} for HX_2 that is extracted from the perpendicularly polarized data in Figure 3C is slightly larger, 1.71 ± 0.08 meV, reflecting the very slight shift of both features *k* and *l* to slightly lower frequencies along the ω_2 axis than the analogous features *a* and *b*.

The HX_2 and MX_2 dephasing times were determined from fits of the Lorentzian line widths of the 2D spectral magnitudes projected to the ω_2 axis for the peaks *a* and *f*, respectively, yielding values of 2.23 ± 0.07 and 1.46 ± 0.07 ps, respectively. The dephasing times also may be determined from the time-dependent transients as shown for HX_2 in Figure 5. We also varied the coherently generated carrier density by changing the average power of the excitation fields. The biexciton dephasing times decreased as the power was increased, revealing excitation-induced biexciton dephasing, which results from six-particle (exciton−biexciton) interactions.

The real parts of the 2D spectral magnitudes of Figure 3 are displayed in Figure 6. The nodes belonging to the two-quantum features are perpendicular to the $y = 2x$ line, consistent with a two-quantum non-rephasing interpretation of the measurements. The real part of the 2D spectrum for the cross-circular excitation case is shown in Figure 6A. The HX_2 peak (*a*) is largely positive, which indicates that the final field, $\vec{E}_C$, stimulated emission from the biexciton to the exciton state. The red-shifted shoulder (*b*), which is due to a biexciton−exciton coherence that evolved during the emission time period, is largely negative, which indicates absorption of a photon from the final field. The vertically elongated feature is in phase with the HX_2 peak. The real part of the 2D spectrum for the cocircular excitation case is shown in Figure 6B. Unlike the HX_2 peak, the interaction-induced coherence peak (*h*) is out of phase with the vertically elongated feature. The vertically elongated feature was previously explained to arise from interaction between an exciton and free electron−hole pair mediated by EID.[34] Since EID and EIS interactions were found to be 90° out of phase, as discussed above, we can conclude that the interaction-induced coherence peak largely results from an EIS interaction between excitons. Phenomenological modeling of EIS and EID contributions to the two-quantum 2D FTOPT spectrum of a two-level system (which represents interactions in an ensemble of exciton states where biexciton contributions are neglected) may reveal the origin of the interaction-induced coherence peak for the cocircular excitation case. In fact, EIS contributions should still be present in the measurements using cross-circular excitation, which may explain the change in the line shapes of *a* and *b* when compared with the line shapes of *k* and *l* in the perpendicularly polarized excitation measurement, shown in Figure 6C, where contributions from many-body effects are largely suppressed.

Conclusions and Outlook

The two-quantum 2D FTOPT measurements presented here permit isolation and elaboration of many-body interactions

Downloaded by RENMIN UNIV OF CHINA on October 2, 2009 | http://pubs.acs.org
Publication Date (Web): August 19, 2009 | doi: 10.1021/ar900122k

Downloaded by RENMIN UNIV OF CHINA on October 2, 2009 | http://pubs.acs.org
Publication Date (Web): August 19, 2009 | doi: 10.1021/ar900122k

that cannot be treated using a mean-field approximation for the prototype GaAs system. The robustness of the spatiotemporal pulse shaping approach simplifies and enhances the execution of these otherwise daunting measurements. By separating coherent signal contributions along another frequency axis, the energetics and dephasing dynamics associated with four-particle correlations can be determined independently of two-particle correlations. Specifically, the biexciton binding energy determined directly from the biexciton−ground-state coherence was shown to differ from the binding energy determined indirectly by comparing the energy of a biexciton−exciton coherence to an exciton−ground-state coherence. Furthermore, a study of the dephasing time of HX_2 and MX_2 biexciton coherences with respect to the coherently generated carrier density reveals a dependence on even higher-order particle correlations. Also, since the full complex signal field is obtained, the observed 2D line shapes can be compared with theoretical predictions of the response in order to determine the dominating microscopic many-body mechanism.

Future works will demonstrate the excitation of six-particle correlations through a $\chi^{(5)}$ process and three-dimensional FTOPT spectroscopic measurements,[31] which discern more of the contributing Feynman pathways. The same apparatus and measurements can be used for feedback-directed quantum control over the coherences. In quantum dots, observation of multiple-quantum coherences and populations from biexcitons and higher-lying states will have additional importance in laser gain, solar energy conversion, and other applications. Also of interest would be exciton and biexciton correlations in J-aggregates where 2D FTOPT could reveal how electronic energy is transferred between different strata of organic photovoltaic cells.

This work was supported in part by the National Science Foundation Grant CHE-0616939. The authors wish to thank X. Li, M. Kira, and D. Jonas for helpful discussions. D. Turner wishes to thank the NDSEG Fellowship Program for financial support.

BIOGRAPHICAL INFORMATION

Katherine W. Stone (Ph.D. Physical Chemistry, MIT, 2009) is a postdoctoral researcher at the Laboratory for Organic Optics and Electronics of MIT.

Daniel B. Turner (B.A. Chemistry and Mathematics 2004, Concordia College−Moorhead) is a graduate student at MIT interested in using high-order spectroscopy experiments and theory to understand many-body correlations of excitons.

Kenan Gundogdu (Ph.D. Physics, University of Iowa, 2004) joined the North Carolina State University Physics Department as an Assistant Professor in 2008. His current research involves electron dynamics in light-harvesting complexes for solar energy conversion and characterization of transition metal oxides using nonlinear optical spectroscopy.

Steven T. Cundiff (Ph.D. Applied Physics, University of Michigan, 1992) is a JILA Fellow, Chief of the NIST Quantum Physics Division, and an Adjoint Assoc. Professor in the Physics and Electrical and Computer Engineering Departments at the University of Colorado. His research interests include femtosecond comb technology and ultrafast spectroscopy of semiconductors and dense atomic vapors.

Keith A. Nelson (Ph.D. Physical Chemistry, Stanford University, 1981) is a professor at the Department of Chemistry of MIT. His research is aimed at time-resolved optical study and coherent control of condensed matter. He has developed femtosecond pulse shaping techniques for multiple-pulse excitation and coherent control of acoustic waves, crystal lattice vibrations, and excitons, which mediate collective structural change and electronic excited-state dynamics in a wide range of materials.

FOOTNOTES

*To whom correspondence should be addressed. E-mail: kanelson@mit.edu.

§Present address: Department of Physics, North Carolina State University, Raleigh, NC 27695.

REFERENCES

1 Engel, G. S.; Calhoun, T. R.; Read, E. L.; Ahn, T.-K.; Mancal, T.; Cheng, Y.-C.; Blankenship, R. E.; Fleming, G. R. Evidence for wavelike energy transfer through quantum coherence in photosynthetic systems. *Nature* **2007**, *446*, 782–786.

2 Abramavicius, D.; Voronine, D. V.; Mukamel, S. Double-quantum resonances and exciton scattering in coherent 2D spectroscopy of photosynthetic complexes. *Proc. Natl. Acad. Sci. U.S.A.* **2008**, *105*, 8525–8530.

3 Klimov, V. I.; Mikhailovsky, A. A.; Xu, S.; Malko, A.; Hollingsworth, J. A.; Leatherdale, C. A.; Eisler, H.-J.; Bawendi, M. G. Optical gain and stimulated emission in nanocrystal quantum dots. *Science* **2000**, *290*, 314–317.

4 Voss, T.; Ruckman, I.; Gutowski, J.; Axt, V. M.; Kuhn, T. Coherent control of the exciton and exciton-biexciton transitions in the generation of nonlinear wave-mixing signals in a semiconductor quantum well. *Phys. Rev. B* **2006**, *73*, 115311.

5 Li, X.; Wu, Y.; Steel, D.; Gammon, D.; Stievater, T. H.; Katzer, D. S.; Park, D.; Piermarocchi, C.; Sham, L. J. An all-optical quantum gate in a semiconductor quantum dot. *Science* **2003**, *301*, 809–811.

6 Manzke, G.; Peng, Q. Y.; Henneberger, K.; Neukirch, U.; Hauke, K.; Wundke, K.; Gutowski, J.; Hommel, D. Density dependence of the exciton energy in semiconductors. *Phys. Rev. Lett.* **1998**, *80*, 4943–4946.

7 Shulthesis, L.; Kuhl, J.; Honold, A.; Tu, C. W. Ultrafast phase relaxation of excitons via exciton-exciton and exciton-electron collisions. *Phys. Rev. Lett.* **1986**, *57*, 1635–1638.

8 Cundiff, S. T. Coherent spectroscopy of semiconductors. *Opt. Exp.* **2008**, *16*, 4639–4664.

9 Axt, V. M.; Kuhn, T. Femtosecond spectroscopy in semiconductors: A key to coherences, correlations and quantum kinetics. *Rep. Prog. Phys.* **2004**, *67*, 433–512.

10 Chemla, D. S.; Shah, J. Many-body and correlation effects in semiconductors. *Nature* **2001**, *411*, 549–557.

11 Miller, R. C.; Kleinman, D. A.; Gossard, A. C.; Munteanu, O. Biexcitons in GaAs quantum wells. *Phys. Rev. B* **1982**, *25*, 6545–6547.

12 Feuerbacher, B. F.; Kuhl, J.; Ploog, K. Biexcitonic contribution to the degenerate-four-wave mixing signal from a GaAs/Al_xGa_{1-x}As quantum well. *Phys. Rev. B* **1991**, *43*, 2439–2441.

13 Munowitz, M.; Pines, A. Multiple-quantum nuclear magnetic resonance spectroscopy. *Science* **1986**, *233*, 525–531.

14 Fulmer, E. C.; Mukherjee, P.; Krummel, A. T.; Zanni, M. T. A pulse sequence for directly measuring the anharmonicities of coupled vibrations: Two-quantum two-dimensional infrared spectroscopy. *J. Chem. Phys.* **2004**, *120*, 8067–8078.

15 Tian, P.; Keusters, D.; Suzaki, Y.; Warren, W. S. Femtosecond phase-coherent two-dimensional spectroscopy. *Science* **2003**, *300*, 1553–1555.

16 Zhang, T.; Kuznetsova, I.; Meier, T.; Li, X.; Mirin, R. P.; Thomas, P.; Cundiff, S. T. Multidimensional ultrafast spectroscopy special feature: Polarization-dependent optical 2D Fourier transform spectroscopy of semiconductors. *Proc. Natl. Acad. Sci. U.S.A.* **2007**, *104*, 14227–14232.

17 Cundiff, S. T.; Zhang, T.; Bristow, A. D.; Karaiskaj, D.; Dai, X. Optical two-dimensional fourier transform spectroscopy of semiconductor quantum wells. *Acc. Chem. Res.* **2009**, *42*, doi: 10.1021/ar9000636.

18 Leo, K.; Wegener, M.; Shah, J.; Chemla, D. S.; Gobel, E. O.; Damen, T.; Schmitt-Rink, S.; Schafer, W. Effects of coherent polarization interactions on time-resolved degenerate four-wave mixing. *Phys. Rev. Lett.* **1990**, *65*, 1340–1343.

19 Wegener, M.; Chemla, D. S.; Schmitt-Rink, S.; Schafer, W. Line shape of time-resolved four-wave mixing. *Phys. Rev. A* **1990**, *42*, 5675–5683.

20 Mayer, E. J.; Smith, G. O.; Heuckeroth, V.; Kuhl, J.; Bott, K.; Schulze, A.; Meier, T.; Bennhardt, D.; Koch, S. W.; Thomas, P.; Hey, R.; Ploog, K. Evidence of biexcitonic contributions to four-wave mixing in GaAs quantum wells. *Phys. Rev. B* **1994**, *50*, 14730–14733.

21 Mukamel, S. *Principles of Nonlinear Optical Spectroscopy*; Oxford University Press, Inc.: New York, 1995.

22 Wang, H.; Ferrio, K.; Steel, D. G.; Hu, Y. Z.; Binder, R.; Koch, S. W. Transient nonlinear optical response from excitation induced dephasing in GaAs. *Phys. Rev. Lett.* **1993**, *71*, 1261–1264.

23 Li, X.; Zhang, T.; Borca, C. N.; Cundiff, S. T. Many-body interactions in semiconductors probed by optical two-dimensional Fourier transform spectroscopy. *Phys. Rev. Lett.* **2006**, *96*, 057406.

24 Wang, H.; Ferrio, K. B.; Steel, D. G.; Berman, P. R.; Hu, Y. Z.; Binder, R.; Koch, S. W. Transient four-wave-mixing line shapes: Effects of excitation-induced dephasing. *Phys. Rev. A* **1994**, *49*, R1551–R1554.

25 Meier, T.; Thomas, P.; Koch, S. W. *Coherent Semiconductor Optics: From Basic Concepts to Nanostructure Applications*; Springer: Berlin; New York, 2007.

26 Chen, G.; Stievater, T. H.; Batteh, E. T.; Li, X.; Steel, D. G.; Gammon, D.; Katzer, D. S.; Park, D.; Sham, L. J. Biexciton quantum coherence in a single quantum dot. *Phys. Rev. Lett.* **2002**, *88*, 117901.

27 Ferrio, K. B.; Steel, D. G. Observation of the ultrafast two-photon coherence biexciton oscillation in a GaAs/$Al_xGa_{1-x}As$ multiple quantum well. *Phys. Rev. B* **1996**, *54*, R5231–R5234.

28 Vaughan, J. C.; Hornung, T.; Feurer, T.; Nelson, K. A. Diffraction-based femtosecond pulse shaping with a two-dimensional spatial light modulator. *Opt. Lett.* **2005**, *30*, 323–325.

29 Vaughan, J. C.; Hornung, T.; Stone, K. W.; Nelson, K. A. Coherently controlled ultrafast four-wave mixing spectroscopy. *J. Phys. Chem. A* **2007**, *111*, 4873–4883.

30 Lepetit, L.; Cheriaux, G.; Joffre, M. Linear techniques of phase measurement by femtosecond spectral interferometry for applications in spectroscopy. *J. Opt. Soc. Am. B* **1995**, *12*, 2467–2474.

31 Turner, D. B.; Stone, K. W.; Gundogdu, K.; Nelson, K. A. Three-dimensional electronic spectroscopy of excitons in GaAs quantum wells, manuscript in preparation.

32 Backus, E. H. G.; Garrett-Roe, S.; Hamm, P. Phasing problem of heterodyne-detected two-dimensional infrared spectroscopy. *Opt. Lett.* **2008**, *33*, 2665–2667.

33 Bristow, A. D.; Karaiskaj, D.; Dai, X.; Cundiff, S. T. All-optical retrieval of the global phase for two-dimensional Fourier-transform spectroscopy. *Opt. Exp.* **2008**, *16*, 18017–18027.

34 Borca, C. N.; Zhang, T.; Li, X.; Cundiff, S. T. Optical two-dimensional Fourier transform spectroscopy of semiconductors. *Chem. Phys. Lett.* **2005**, *416*, 311–315.

35 Pantke, K.-H.; Oberhauser, D.; Lyssenko, V. G.; Hvam, J. M.; Weimann, G. Coherent generation and interference of excitons and biexcitons in GaAs/AlGaAs quantum wells. *Phys. Rev. B* **1993**, *47*, 2413–2416.

Downloaded by RENMIN UNIV OF CHINA on October 2, 2009 | http://pubs.acs.org
Publication Date (Web): August 19, 2009 | doi: 10.1021/ar900122k